Research Square

Preprints are preliminary reports that have not undergone peer review.
They should not be considered conclusive, used to inform clinical practice,
or referenced by the media as validated information.

Interfacial Regulation of Ruthenium Oxide-Modified CeVO4 Catalysts for the Catalytic Oxidation of Ammonia

Shuangye Li
State Key Laboratory of Iron and Steel Industry Environmental Protection, Central Research Institute of Building and Construction, Co., Ltd, MCC Group

Hui Wang
State Key Laboratory of Iron and Steel Industry Environmental Protection, Central Research Institute of Building and Construction, Co., Ltd, MCC Group

Jiahao Chen
State Key Laboratory of Iron and Steel Industry Environmental Protection, Central Research Institute of Building and Construction, Co., Ltd, MCC Group

Xiaochen Xun
State Key Laboratory of Iron and Steel Industry Environmental Protection, Central Research Institute of Building and Construction, Co., Ltd, MCC Group

Yuan Dong
State Key Laboratory of Iron and Steel Industry Environmental Protection, Central Research Institute of Building and Construction, Co., Ltd, MCC Group

Mengxin Li
State Key Laboratory of Iron and Steel Industry Environmental Protection, Central Research Institute of Building and Construction, Co., Ltd, MCC Group

Hui Peng
China South To North Water Diversion Group Ecological Environmental Protection Co., Ltd

Meiling Cao
State Key Laboratory of Iron and Steel Industry Environmental Protection, Central Research Institute of Building and Construction, Co., Ltd, MCC Group

Hongxing Dai
Department of Chemical Engineering and Technology, College of Materials Science and Engineering, Beijing University of Technolog

Wenbo Zhang
zhangwenbo@cribc.com

State Key Laboratory of Iron and Steel Industry Environmental Protection, Central Research Institute of Building and Construction, Co., Ltd, MCC Group

Xiaohua Zhu
State Key Laboratory of Iron and Steel Industry Environmental Protection, Central Research Institute of Building and Construction, Co., Ltd, MCC Group

Research Article

Keywords: NH3-SCO, CeVO4, RuOx, metal-support interaction, i-SCR mechanism

Posted Date: November 9th, 2026

DOI: https://doi.org/10.21203/rs.3.rs-11438473/v1

License: This work is licensed under a Creative Commons Attribution 4.0 International License.
Read Full License

Additional Declarations: No competing interests reported.

Interfacial Regulation of Ruthenium Oxide-Modified $CeVO_4$ Catalysts for the Catalytic Oxidation of Ammonia

Shuangye Li[ab], Hui Wang[a], Jiahao Chen[a], Xiaochen Xun[a], Yuan Dong[a], Mengxin Li[a], Hui Peng[c], Meiling Cao[a], Hongxing Dai[b], Wenbo Zhang*[a] and Xiaohua Zhu*[a]*

[a] *State Key Laboratory of Iron and Steel Industry Environmental Protection, Central Research Institute of Building and Construction, Co., Ltd, MCC Group, Beijing, 100088, China.*

[b]*Department of Chemical Engineering and Technology, College of Materials Science and Engineering, Beijing University of Technology, Beijing 100124, China.*

[c]*China South To North Water Diversion Group Ecological Environmental Protection Co., Ltd. Beijing 102300, China.*

*E-mail: zhuxiaohua@cribc.com

hxdai@bjut.edu.cn

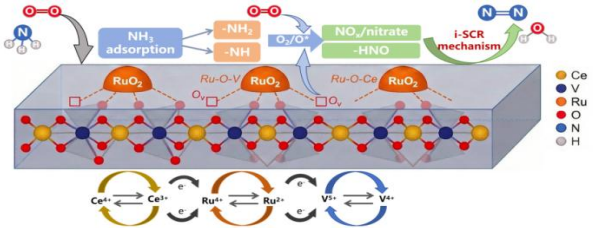
zhangwenbo@cribc.com

ABSTRACT

The selective catalytic oxidation of ammonia (NH_3-SCO) to nitrogen (N_2) is an effective strategy for controlling NH_3 slip emissions from selective catalytic reduction (SCR) systems. This study reports the synthesis of $CeVO_4$ by microwave-assisted deposition-precipitation and the preparation of RuO_x-modified $CeVO_4$ catalysts (xRu/$CeVO_4$, x = 0-3 wt%) via wet impregnation, along with a systematic evaluation of the influence of RuO_x loading on the NH_3-SCO reaction performance. The results demonstrated that the incorporation of RuO_x significantly enhanced the low-temperature catalytic activity of the pristine $CeVO_4$ catalyst. The 2Ru/$CeVO_4$ catalyst exhibited the best overall activity, achieving complete NH_3

conversion at 240 °C, whereas the pristine $CeVO_4$ reached only 98.5% NH_3 conversion even at 320 °C. Comprehensive characterization by XRD, TEM, NH_3-TPD, H_2-TPR, XPS, and *in situ* DRIFTs revealed that the improved performance originates from strong metal-support interactions (SMSI) between RuO_x and the $CeVO_4$ support. At the optimal loading, the introduction of Ru increased the surface chemisorbed oxygen (O_α) content and the number and strength of acid sites. The Ru-O-V and Ru-O-Ce interfacial architectures substantially accelerated low-temperature NH_3 oxidation; however, the strong oxidizing ability of RuO_x lowered the N_2 selectivity of all the Ru-containing samples with respect to the pristine support and made it decrease further with temperature, which reveals an intrinsic activity-N_2 selectivity trade-off. These findings provide mechanistic insight into the role of RuO_x in $CeVO_4$-based NH_3-SCO catalysts and offer rational guidance for the development of high-performance NH_3 abatement materials.

Graphical Abstract



Keywords: NH_3-SCO; $CeVO_4$; RuO_x; metal-support interaction; *i*-SCR mechanism

1. Introduction

Ammonia (NH_3) is a hazardous and pungent gaseous pollutant that poses significant threats to human health and the environment[1]. The primary sources of NH_3 emissions include agricultural activities, industrial processes, and, notably, the slip from selective

catalytic reduction (SCR) units used for NO_x abatement in stationary and mobile sources[2]. With the enforcement of increasingly stringent emission regulations worldwide, the development of efficient technologies for ammonia abatement has become an urgent environmental priority.

Among various approaches, the selective catalytic oxidation of ammonia to nitrogen and water (NH_3-SCO) is considered one of the most effective techniques for eliminating gaseous NH_3 emissions. The key challenge in NH_3-SCO lies in achieving both high NH_3 conversion at low temperatures and high selectivity toward N_2. Noble metal-based catalysts, including Pt, Ag, Ru, Ir, Pd, Au, and Rh, have been widely investigated for this reaction due to their satisfactory low-temperature ammonia oxidation activity[3]. Among these, ruthenium Ru-based catalysts have attracted considerable attention owing to their unique intrinsic properties and promising catalytic performance[4]. The RuO_2 phase has been shown to possess exceptionally high intrinsic oxidation activity toward NH_3, enabling complete conversion at relatively low temperatures[5]. For example, RuO_2-modified systems (e.g., $RuO_2/SnTiO_2$, Ru/TiO_2) can achieve near-complete NH_3 conversion below 250-300 ° C [6]. Nevertheless, the strong oxidizing ability of RuO_2 is a double-edged sword: at elevated temperatures, it tends to over-oxidize NH_3 and intermediates into NO_x byproducts, thereby diminishing N_2 selectivity[7]. Recent studies have demonstrated that modulating the surface acidity, oxygen vacancies, and metal-support interactions (MSI) of Ru-based catalysts can effectively balance activity and selectivity. For instance, Nb_2O_5-modified $RuO_2/Sn_{0.2}Ti_{0.8}O_2$ catalysts showed improved N_2 selectivity by tuning the surface

acid sites around the Ru active centers[8]. Similarly, our previous study verified that doping CeO_2 into Ru/TiO_2 can promotes the dispersion of Ru species, forms Ru-O-Ce bonds, and significantly enhance the NH_3-SCO performance of the catalyst[9].

Cerium vanadate ($CeVO_4$), with a tetragonal zircon-type crystal structure, has attracted growing attention as a multifunctional support or active component for SCR and related catalytic reactions. The unique structural features of $CeVO_4$, through the synergistic effect of Ce^{4+}/Ce^{3+} and V^{5+}/V^{3+} redox pairs, endow the material with abundant redox active sites. Strong electron transfer between adjacent V and Ce species ($V^{4+}+Ce^{4+} \leftrightarrow V^{5+}+Ce^{3+}$) has been shown to enhance the redox properties and, consequently, the catalytic performance in NO_x reduction[10-11]. Research indicates that the surface properties and catalytic activity of $CeVO_4$ catalysts are highly tunable by controlling synthesis conditions such as pH and hydrothermal temperature, which directly regulate the vanadium species distribution, surface acidity, and exposed active sites[12]. In addition, our previous study explored a novel microwave-assisted deposition-precipitation method for preparing $NdVO_x/TiO_2$ catalysts. This approach not only enhanced the catalytic performance but also reduced the complexity and energy consumption of the preparation process, offering new insights for the synthesis of vanadates[13].

In this work, a series of xRu/$CeVO_4$ catalysts (x=0-3 wt%) were synthesized microwave-assisted deposition-precipitation and aqueous impregnation, and

their catalytic performance for NH_3-SCO was evaluated. The physicochemical properties of the catalysts were systematically characterized by X-ray diffraction (XRD), H_2 temperature-programmed reduction (H_2-TPR), NH_3 temperature-programmed desorption (NH_3-TPD), transmission electron microscopy (TEM), X-ray photoelectron spectroscopy (XPS), and in situ diffuse reflectance infrared Fourier transform spectroscopy (*in situ* DRIFTs). The promotional role of RuO_x loading on the activity, N_2 selectivity, and reaction mechanism of $CeVO_4$-based catalysts was investigated in detail, with the goal of elucidating structure-activity relationships and providing a rational basis for the design of efficient NH_3-SCO catalysts.

2. Materials and methods

2.1 Materials

NH_4VO_3 (AR), $RuCl_3$•$3H_2O$ (AR) and $Ce(NO_3)_3$•$6H_2O$ (AR) were purchased from Beijing Chemical Works. All other chemicals were received from commercial sources and used without further purification.

2.2 Catalyst preparation

2.2.1 Synthesis of $CeVO_4$ catalyst.

$CeVO_4$ catalyst was prepared by a microwave-assisted deposition-precipitation method. Firstly, a certain amount of $Ce(NO_3)_3$•$6H_2O$ and NH_4VO_3 were dissolved in 100 and 80 mL of deionized water, respectively. Later, PEG-3000 was added into the above $Ce(NO_3)_3$ aqueous solution under stirring 70 ℃. After 60 min, the NH_4VO_3 solution was dropwise

added into the obtained mixture. Subsequently, the suspension was transferred to a microwave oven (80 ℃, 500 W) and heated to boiling until evaporation of the liquid was complete. Then, the resulting paste was dried and calcined in air at 500 ℃ for 3 h (Fig. 1).

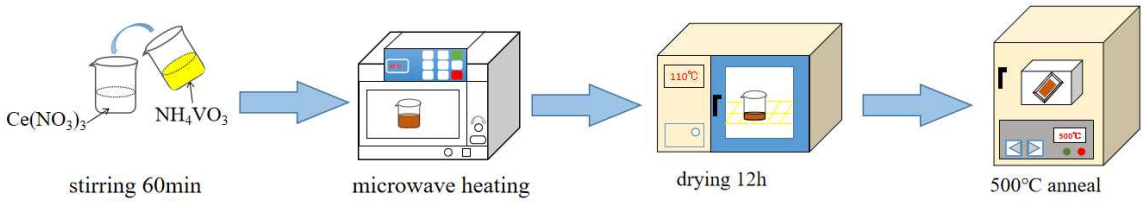


Fig. 1 Process of preparation of the $CeVO_4$ catalyst.

2.2.2 Synthesis of *x*Ru/$CeVO_4$ catalysts.

*x*Ru/$CeVO_4$ (*x*=0%, 1%, 2%, 3%) catalysts were prepared via aqueous impregnation. 9.9 g of $CeVO_4$ support was impregnated with a $RuCl_3$ aqueous solution to load the Ru species. Then the mixture was dried overnight at 110 ℃ and calcined at 500 ℃ for 3 h in air. The resulting catalysts were denoted as "*x*Ru/$CeVO_4$". Finally, all of the catalysts were pressed into pellets and sieved to 40 ~ 60 mesh before use.

2.3 Catalytic Performance Evaluation

A fixed-bed quartz reactor was used for NH_3-SCO activity measurements of the $CeVO_4$ and *x*Ru/$CeVO_4$ catalysts in a steady-state flow mode with 1 mL catalyst (40-60 mesh). Reaction conditions were as follows: 100 ppm NH_3, 5 vol% O_2, and pure N_2 as the balance gas. The total flow rate of the feed gas was 2 L min^{-1}, and the gas hourly space velocity (GHSV) was 1.2×10^5 h^{-1}. After the reaction reached a stable condition for 30 min at every testing temperature, the concentrations of NH_3 and the gas mixture in the reactor outlet included NO, NO_2, and N_2O determined by an exhaust gas analyzer (Gasmet DX 4000 FTIR

Analyzer). The NH_3 conversions were calculated based on the concentrations of the inlet and outlet gas at steady state as the following Eq. (1):

$$NH_3\ Conversion\ (\%)=([NH_3]_{in}-[NH_3]_{out})/[NH_3]_{in}\times 100\% \quad (1)$$

The N_2 selectivity, NO_x (NO, NO_2) yield and N_2O yield in SCO reaction were calculated using the Eqs. (2)-(4):

$$N_2\ Selectivity(\%)=([NH_3]_{in}-[NH_3]_{out}-[NO]_{out}-[NO_2]_{out}-2[N_2O]_{out})/([NH_3]_{in}-[NH_3]_{out})\times 100\% \quad (2)$$

$$NO_x\ yield\ (\%)=([NO]_{out}+[NO_2]_{out})/[NH_3]_{in}\times 100\% \quad (3)$$

$$N_2O\ yield\ (\%)=(2[N_2O]_{out})/[NH_3]_{in}\times 100\% \quad (4)$$

Where the "*in*" and "*out*" were the inlet and outlet of the reactor, respectively.

2.4 Catalyst Characterization

The crystal structures of the catalysts were determined by an X-ray diffractometer (Bruker/AXS D8 Advance) operating at 50 kV and 50 mA using Cu Kα radiation (λ=1.54 Å). The samples were scanned from 10 to 80° (2θ) with a step size of 0.02°.

Scanning electron microscopy (SEM) measurements were obtained on an JSM-7401F instrument, and the transmission electron microscopy (TEM) images were captured using a transmission electron microscope (JEM-2100F).

H_2 temperature-programmed reduction (H_2-TPR) was conducted on a chemisorption analyzer (Micromeritics, AutoChen II 2920). First, 0.10 g of the sample was pretreated in air at 400 ℃ for 30 min before it was cooled down to room temperature. The sample was then purged in an Ar atmosphere until the baseline by heating the sample from 30 to 800 ℃ in a flow of 5 vol% H_2/Ar (50 mL min^{-1}) with a temperature ramp of 10 ℃ min^{-1}. The reducing

gas was cooled in a bath of mixture of isopropanol and liquid nitrogen to condense the water generated during the TPR process. A thermal conductivity detector (TCD) was used to monitor H_2 consumption.

Temperature-programmed desorption of ammonia (NH_3-TPD) measurements were performed on a TP-5080 automated chemisorption analyzer (Tianjin Xianquan Industry and Trade Development Co.,Ltd.). Then, 100mg of each catalyst was loaded in a quartz reactor and preheated at 400 ℃ by O_2/He (20 vol%) for 30 min and subsequently cooled down to 30 ℃. Afterward, the catalyst was saturated with NH_3/He (2 vol%) for 30 min at the same temperature and then flushed with He for 30 min to remove the physically adsorbed NH_3. Finally, the TPD curve was recorded from 30 to 850 ℃ at the rate of 10 ℃/min in He.

X-ray photoelectron spectroscopy (XPS) analyses of the catalysts were conducted using K-Alpha (Thermo Scientific). Before analysis, the samples were calcined in air (labeled as "O") and 5 vol% H_2/Ar (labeled as "H") at 500 ℃.

In situ diffusion Fourier transform infrared spectroscopy (DRIFTs) measurements were performed on a Bruker Tensor II with an MCT detector cooled with liquid nitrogen. The measurements included NH_3 adsorption and transient reactions (i.e. the reaction between O_2 and pre-adsorbed NH_3 species, and the co-feeding of NH_3+O_2 through the catalysts) over the $CeVO_4$ and 2Ru/$CeVO_4$ catalysts. The samples were pretreated at 300 ℃ for 30 min in a flow of N_2 (50 mL min^{-1}) and then cooled down to the desired temperature. The background spectra were collected in flowing N_2 and subtracted from the sample spectra. The following reaction conditions were used: 500 ppm NH_3, 5 vol% O_2, and the balance of the gas was N_2. For each sample, the NH_3 adsorption time was 40 min, followed by N_2 purging for another

30 min until the infrared spectroscopy signals were stabilized. Afterward, NH_3+O_2 were co-fed to the fresh samples at room temperature for 35 min, and the temperature was then raised stepwise to 100, 200, 300 and 350 °C under the same feed, spectra being recorded at each temperature. All spectra were recorded by accumulating 100 scans at a resolution of 4 cm^{-1}.

3. Results and Discussion

3.1 NH_3-SCO performance

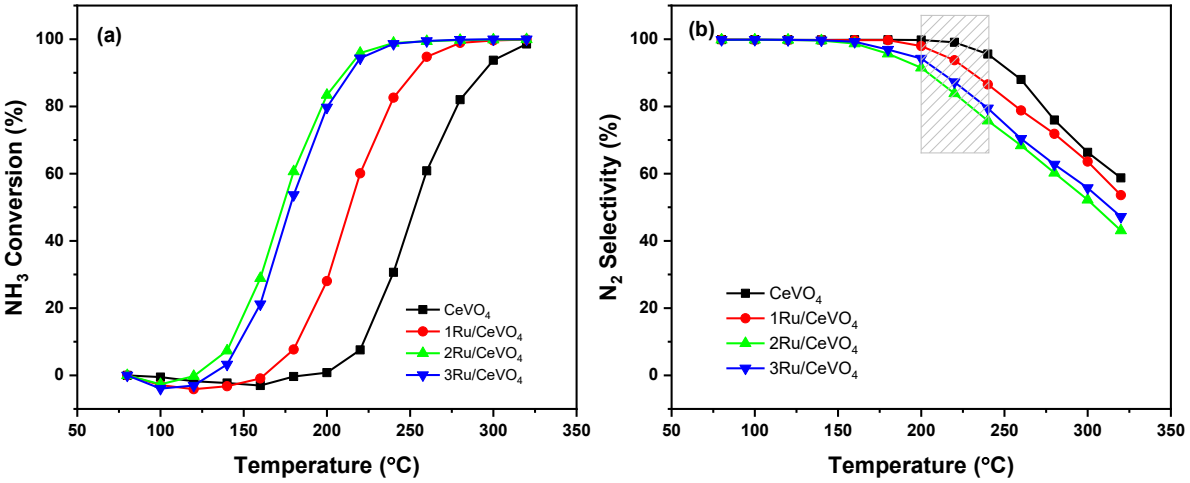


Fig. 2 NH_3-SCO performance of $CeVO_4$ and *x*Ru/$CeVO_4$ catalysts; (a) NH_3 conversion, (b) N_2 selectivity. Reaction conditions: [NH_3]=100 ppm, [O_2]=5 vol%, balance N_2, total flow rate= 2 L min^{-1}, GHSV=1.2×10^5 h^{-1}.

The catalytic activities of the *x*Ru/$CeVO_4$ and $CeVO_4$ catalysts for the NH_3-SCO reaction are shown in Fig. 2(a). The NH_3 conversion over all catalysts increased with increasing temperature. The pristine $CeVO_4$ catalyst was active only in the high-temperature region: its NH_3 conversion remained below 10% up to 220 °C and reached 98.54% only at 320 °C, so that complete NH_3 conversion was not attained within the investigated temperature window.

Compared with the $CeVO_4$ catalyst, the addition of Ru obviously improved the activity of the catalysts. With increasing RuO_x loading from 1 wt% to 2 wt%, the NH_3 conversion increased markedly in the range of 180-280 ℃; at 220 ℃, for instance, it rose from about 8% over $CeVO_4$ to about 60% over $1Ru/CeVO_4$ and about 96% over $2Ru/CeVO_4$. The temperatures required for complete NH_3 conversion (T_{100}) were 280 and 240 ℃ over $1Ru/CeVO_4$ and $2Ru/CeVO_4$, respectively. Further increasing the loading to 3 wt% brought no additional benefit: the NH_3 conversion over $3Ru/CeVO_4$ was slightly lower than that over $2Ru/CeVO_4$ over the whole temperature range, and the activity therefore followed the order of $2Ru/CeVO_4 > 3Ru/CeVO_4 > 1Ru/CeVO_4 > CeVO_4$. Such a non-monotonic dependence on the Ru content indicates that the low-temperature activity is governed by the dispersion of the RuO_x species rather than by their total amount. It was clearly that RuO_x could improve the catalytic activity of $CeVO_4$ obviously in the low temperature range.

The N_2 selectivity of different catalysts was calculated and shown in Fig. 2(b). For all samples the N_2 selectivity decreased monotonically with increasing temperature, and the Ru-containing catalysts were always less selective than the pristine support. At 240 ℃ the N_2 selectivity followed the order of $CeVO_4$ (95.7%) > $1Ru/CeVO_4$ (86.6%) > $3Ru/CeVO_4$ (79.6%) > $2Ru/CeVO_4$ (75.8%). The N_2 selectivity therefore does not decrease monotonically with the Ru loading: the most active sample ($2Ru/CeVO_4$) is the least selective one, whereas $3Ru/CeVO_4$ is slightly more selective than $2Ru/CeVO_4$, in line with its slightly lower NH_3 oxidation activity. The loss of N_2 selectivity is mainly caused by the larger amounts of NO_x (NO, NO_2) by-products formed over the Ru-containing samples, as shown in Fig. S1(a-b). Research findings indicate that the RuO_2 species exhibits significant

oxidation capability[6], which may lead to the formation of NO_x by-products at high temperature in the NH_3-SCO reaction.

3.2 SEM and TEM Results

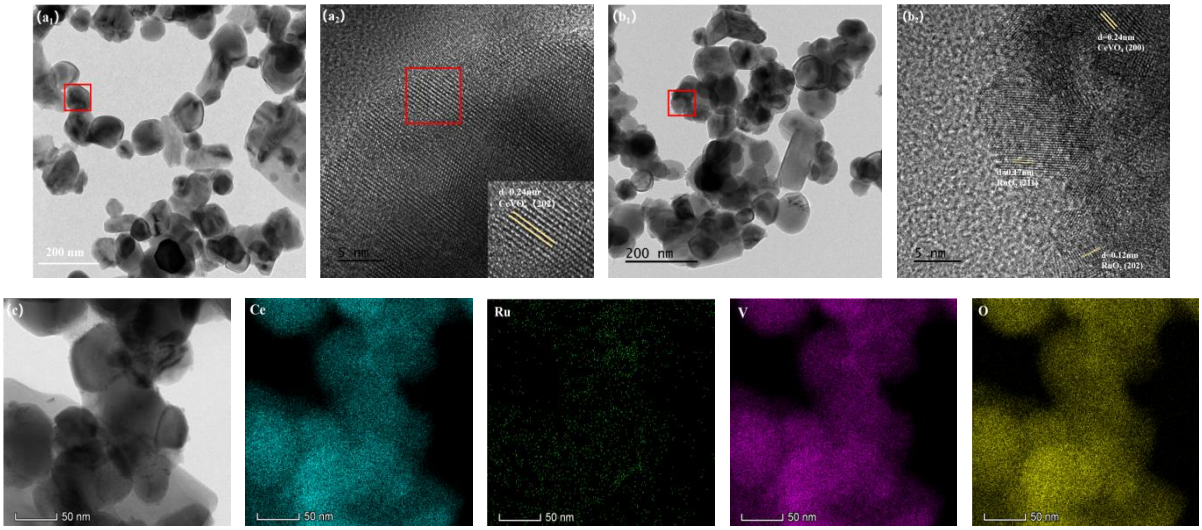


Fig. 3 (a)-(d) TEM images at different magnification of the $CeVO_4$ and $2Ru/CeVO_4$ and (c) EDS elemental mapping of the $2Ru/CeVO_4$ catalyst.

The morphology and size of the obtained samples were examined by SEM and the images were presented in Fig. S2. As shown in Fig. S2(a), $CeVO_4$ catalyst was composed of small spherical particles, indicating microwave-assisted deposition-precipitation method was prone to produce $CeVO_4$ particle with more uniform distribution. For the $2Ru/CeVO_4$ catalysts (Fig. S2(b)), no separate Ru-containing crystallites can be discerned on the surface, which agrees with the high dispersion of the RuO_2 nanocrystallites revealed by XRD and TEM. The images show that the impregnation does not alter the spherical morphology of the support. The uniform and well-dispersed particles expose more accessible active sites for the adsorption of the reaction gases (NH_3 and O_2), which is favourable for the SCO reaction.

Fig. 3 present the electron microscopic images at different magnification for $CeVO_4$ and

227 2Ru/$CeVO_4$. The high-resolution TEM (HRTEM) analysis provides further insight into the
228 crystalline phases of the composites. As depicted in Fig. 3(a_2), well-resolved lattice fringes
229 with an interplanar spacing of 0.24 nm are observed, which are unambiguously indexed to
230 the (202) crystalline plane of the tetragonal zircon-type $CeVO_4$ phase (JCPDS No. #12-0757).
231 The TEM test results can prove that the catalyst indicates the vanadate production under the
232 preparation method. For the 2Ru/$CeVO_4$ sample, the HRTEM image (Fig. 3b_2) clearly
233 distinguishes the presence of additional nano-crystallites on the $CeVO_4$ surface.
234 Characteristic lattice spacings of 0.17 nm and 0.12 nm are respectively identified as the (211)
235 and (202) facets of the RuO_2 phase, providing direct evidence of the successful anchoring
236 and crystallization of ruthenium oxide onto the vanadate support. Furthermore, elemental
237 mapping was applied to detect the distribution of elements contained in the catalyst, and the
238 result is shown in Fig. 3(c). The Ce, V, O and Ru signals overlap and are uniformly
239 distributed over the whole particle, confirming that the Ru species are homogeneously
240 dispersed on the $CeVO_4$ support.

3.3 XRD Results

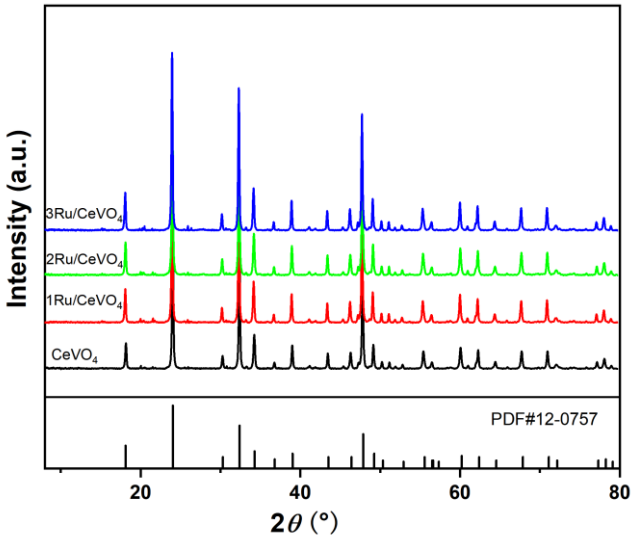


Fig. 4 XRD spectra of the $CeVO_4$ and *x*Ru/$CeVO_4$ catalysts.

The XRD spectra of the *x*Ru/$CeVO_4$ catalysts and pure $CeVO_4$ are presented in Fig. 4. All catalysts show distinct diffraction peaks at 2θ = 18.1, 24.0, 30.3, 32.4, 34.3, 39.0, 43.5, 46.4, 47.9, 49.2, 55.5, 56.5, 60.2, 62.4, 67.9, and 71.1°, which suggested the presence of tetragonal $CeVO_4$ phase (JCPDS #12-0757). The well-defined and relatively sharp diffraction peaks suggest that the $CeVO_4$ support possesses good crystallinity. Notably, for all Ru/$CeVO_4$ catalysts, no diffraction peaks attributable to metallic Ru or ruthenium oxide (RuO_x) crystalline phases are detected, even when the Ru loading is increased from 1 wt% to 3 wt%. The absence of Ru-related reflections strongly indicates that the Ru species are highly dispersed on the $CeVO_4$ support surface, existing either as amorphous phases or as ultra-fine nanoparticles below the detection limit of XRD. This high dispersion state is crucial for maximizing the number of accessible active sites and is generally considered beneficial for enhancing the catalytic performance in NH_3 oxidation reactions[14].

3.4 NH_3-TPD

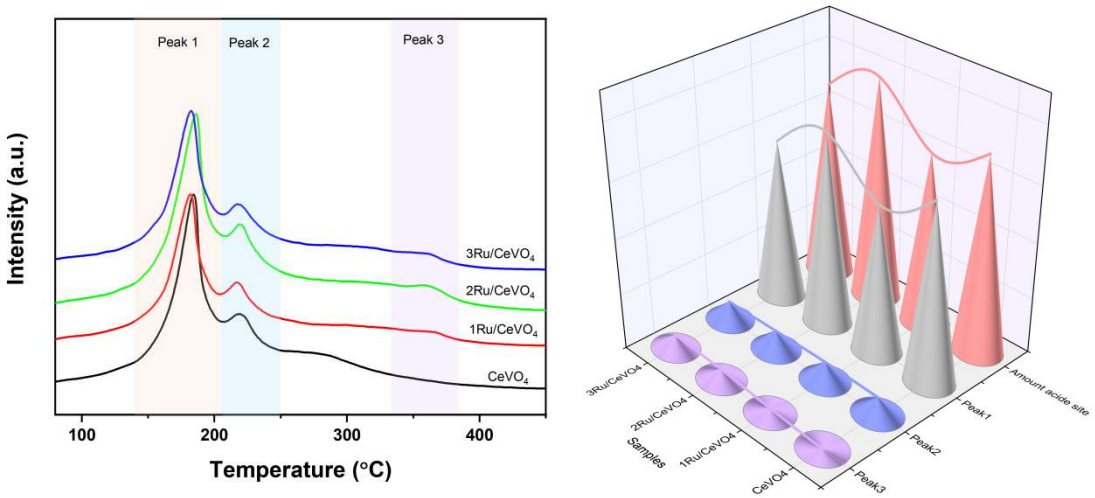


Fig. 5 NH_3-TPD profiles of $CeVO_4$ and *x*Ru/$CeVO_4$ catalysts

Fig. 5a presents the NH_3 temperature-programmed desorption (NH_3-TPD) profiles of the pristine $CeVO_4$ and *x*Ru/$CeVO_4$ catalysts. It is well established that ammonia adsorbed on Brønsted acid sites desorbs at lower temperatures than that on Lewis acid sites. Accordingly, the profiles were divided into three desorption regions: below 200 °C (weak acid site, assigned to NH_4^+ bound to Brønsted acid sites), 200-300 °C (weak-to-medium acid sites) and 300-400 °C (medium-strength acid site, assigned to NH_3 coordinated to Lewis acid sites)[15]. All the samples exhibit two overlapping desorption maxima at about 185 and 220 ℃ together with a broad feature centred at around 355 ℃. Fig. 5b presents the quantitative analysis of acid site concentrations, with the amounts of weak, medium, and total acid sites on the catalyst surfaces calculated from the integrated areas of the NH_3 desorption signals.

The results reveal that the concentration of weak acid sites varies non-monotonically with the Ru loading, first decreasing and then increasing, while the 2Ru/$CeVO_4$ catalyst possesses the highest total acid site concentration among all the sample. More notably, the

incorporation of Ru markedly intensifies the desorption feature in the 300-400 ℃ region, which corresponds to medium-strength acid sites and is only weakly developed on the pristine $CeVO_4$ sample. This observation indicates that Ru modification effectively enhances both the quantity and strength of Lewis acid sites on the catalyst surface. These findings are consistent with literature reports demonstrating that Ru introduction can effectively modulate the surface acidity of oxide catalysts. For instance, in Ru-Ce-Zr bifunctional catalyst systems, strong interactions between Ru and Ce species have been shown to significantly increase the population of both Lewis and Brønsted acid sites[16-17]. This is also in agreement with the *in situ* DRIFTs results discussed below, where both the NH_4^+ bands of the Brønsted acid sites and the coordinated NH_3 bands of the Lewis acid sites are more intense on $2Ru/CeVO_4$ than on the pristine $CeVO_4$. The enhanced surface acidity facilitates NH_3 adsorption and activation, which in turn exerts a critical influence on the NH_3-SCO catalytic performance.

3.5 H_2-TPR

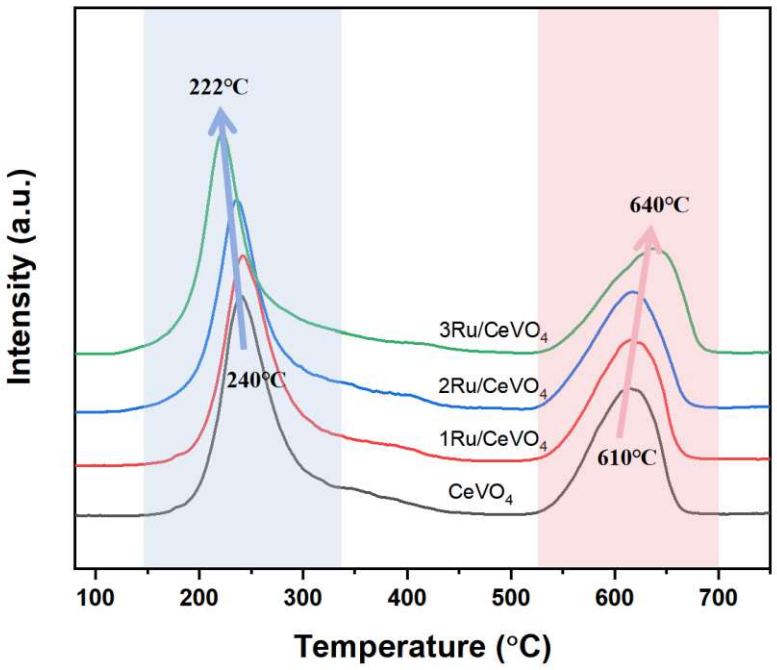


Fig. 6 H_2-TPR profiles of $CeVO_4$ and *x*Ru/$CeVO_4$ catalysts

Fig. 6 displays the H_2-TPR profiles of the pristine $CeVO_4$ and *x*Ru/$CeVO_4$ catalysts. Two distinct reduction peaks are observed for all samples: a low-temperature peak in the range of 200-300 °C and a high-temperature peak centered at approximately 600 °C. For the pristine $CeVO_4$, the low-temperature peak (about 240 °C) is assigned to the reduction of surface Ce^{4+} together with the removal of surface lattice oxygen, whereas the high-temperature peak corresponds to the bulk reduction of V^{5+} to lower valence states[18-19]. However, upon the introduction of Ru, the low-temperature peak shift progressively toward lower temperatures. Previous studies have shown that this low-temperature peak may also involve the reduction of Ru-O-Ce bonds (oxygen bridge); such oxygen bridges are weakly bonded and readily reduced at low temperatures[20]. The introduction of Ru facilitates the cleavage of Ce-O bonds at adjacent sites, thereby activating both surface and lattice oxygen of the support and promoting the formation of Ru-O-Ce bonds. This phenomenon also fully demonstrates that the introduction of Ru species can enhance the low-temperature redox ability of the catalyst. The activated hydrogen atoms dissociated on Ru sites readily migrate to the adjacent $CeVO_4$ support, greatly facilitating the reduction of surface Ce/V cations at lower temperatures[21]. Moreover, the incorporation of Ru cations into the $CeVO_4$ lattice or their intimate contact with the support may create additional oxygen vacancies and structural defects, further improving the mobility of surface oxygen and the overall redox properties[22]. It should be stressed, however, that the largest low-temperature shift is obtained on 3Ru/$CeVO_4$, which is not the most active sample. The low-temperature reducibility probed by H_2-TPR is therefore not the only descriptor of the NH_3-SCO activity, which also depends on the dispersion of the

RuO_x species and on the surface acidity.

In contrast, the high-temperature peak remains essentially unchanged (about 620 °C) for 1Ru/$CeVO_4$ and 2Ru/$CeVO_4$, but shifts to about 642 °C when the Ru loading is further increased to 3 wt%. This implies that the bulk reducibility becomes more difficult at higher Ru loadings. This phenomenon can be rationalized as follows: at higher Ru loadings, the excessive Ru species tend to agglomerate into larger RuO_2 particles rather than maintaining a highly dispersed state[23]. The formation of agglomerated RuO_2 particles significantly hinders the outward migration of bulk lattice oxygen, thereby inhibiting the deep reduction of bulk V^{5+} and Ce^{4+} species and necessitating a higher temperature for completion. At an optimal loading, in contrast, the strong interaction between Ru and the Ce/V species keeps the RuO_x species highly dispersed and preserves the fast transport of lattice oxygen[24]. These results demonstrate that an appropriate Ru loading is essential for optimizing the redox properties of $CeVO_4$-based catalysts. The enhanced reducibility and oxygen mobility achieved at optimal Ru loading are beneficial for the NH_3-SCO reaction, as they facilitate the activation of oxygen species and the subsequent oxidation of adsorbed NH_3.

3.6 XPS Results

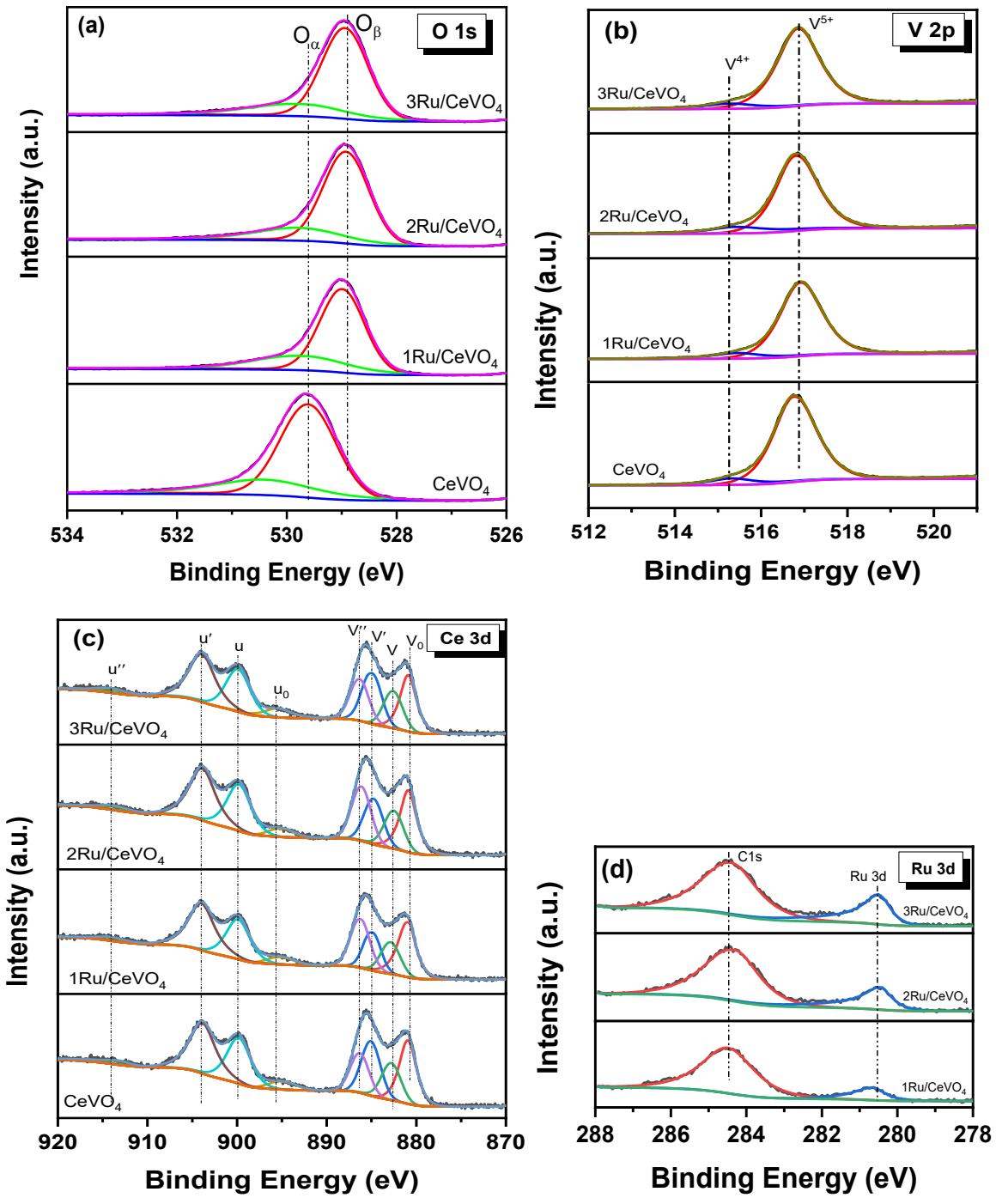


Fig. 7 XPS spectra of (a) O 1s; (b) V 2p ; (c) Ce 3d and (d) Ru 3d of $CeVO_4$ and *x*Ru/$CeVO_4$ catalysts.

Table 1 Results of the O1s, V2p and Ce^{4+} ananlysis of $CeVO_4$ and *x*Ru/$CeVO_4$ catalysts.

Sample	$O_\alpha/(O_\alpha+O_\beta)$	$V^{5+}/(V^{4+}+V^{5+})$	$Ce^{4+}/(Ce^{3+}+Ce^{4+})$

$CeVO_4$	22%	30%	43%
1Ru/$CeVO_4$	26%	29%	46%
2Ru/$CeVO_4$	27%	27%	47%
3Ru/$CeVO_4$	22%	28%	44%

X-ray photoelectron spectroscopy (XPS) was conducted to investigate the surface elemental composition, chemical states, and interfacial electronic interactions of the pristine $CeVO_4$ and *x*Ru/$CeVO_4$ catalysts. The high-resolution spectra of O 1s, V 2p, Ce 3d, and Ru 3d are depicted in Fig. 7, with the corresponding quantitative data summarized in Table 1.

The XPS spectra of O1s of the pure $CeVO_4$ and *x*Ru/$CeVO_4$ catalysts are shown in Fig. 7 (a). For all samples, the O1s peaks can be deconvoluted into two primary distinct peaks. The first peak, which has a lower binding energy of 529.5eV, is attributed to the lattice oxygen (O_β)[25]. The overlapping peaks of O1s with binding energy of 531 eV was attributed to surface adsorbed oxygen (O_α)[26]. The surface chemisorbed oxygen (O_α) has been reported to be the most active oxygen in the oxidation reaction due to its higher mobility compared to lattice oxygen (O_β)[27]. As shown in Table 1, the ratio of $O_\alpha/(O_\alpha+O_\beta)$ rises from 22% for pristine $CeVO_4$ to 27% for 2Ru/$CeVO_4$, indicating that the incorporation of Ru species facilitates the formation of surface oxygen vacancies, which is consistent with the enhanced low-temperature reducibility observed by H_2-TPR and can be rationalised by the strong metal-support interaction (SMSI) at the Ru-O-V and Ru-O-Ce interfaces perturbing the local coordination environment of the $CeVO_4$ lattice. However, a further increase in Ru loading to 3Ru/$CeVO_4$ results in a decrease of the O_α ratio back to 22%, presumably due to the agglomeration of Ru nanoparticles. The coverage of the $CeVO_4$ surface by these particles reduces the number of accessible interfacial sites at which chemisorbed oxygen is stabilised.

Fig. 7(b) shows XPS spectra of V 2p of the catalysts. The center of the peak binding energy of the catalysts exists at 515.3 and 516.7 eV. According to the handbook of the elements and native oxides for XPS, the catalysts possess the V^{5+} peak binding energy at 516.7 eV and the V^{4+} peak binding energy at 515.3 eV[28]. Notably, the $V^{5+}/(V^{4+}+V^{5+})$ ratios listed in Table 1 are only 27-30% for all samples, indicating that the surface vanadium is predominantly in the V^{4+} state. Upon the introduction of Ru, the ratio slightly decreases from 30% for pristine $CeVO_4$ to 27% for $2Ru/CeVO_4$. Since all samples were subjected to the same pretreatment procedure, this decrease can be attributed to the variation in Ru loading. The Ru species are likely to facilitate electron transfer at the Ru-O-V interface, thereby partially reducing the surface V^{5+} to V^{4+}. This valence variation suggests that the introduction of Ru species promotes the reducibility of the vanadium sites, facilitating the redox cycles essential for the selective catalytic oxidation (SCO) of NH_3.

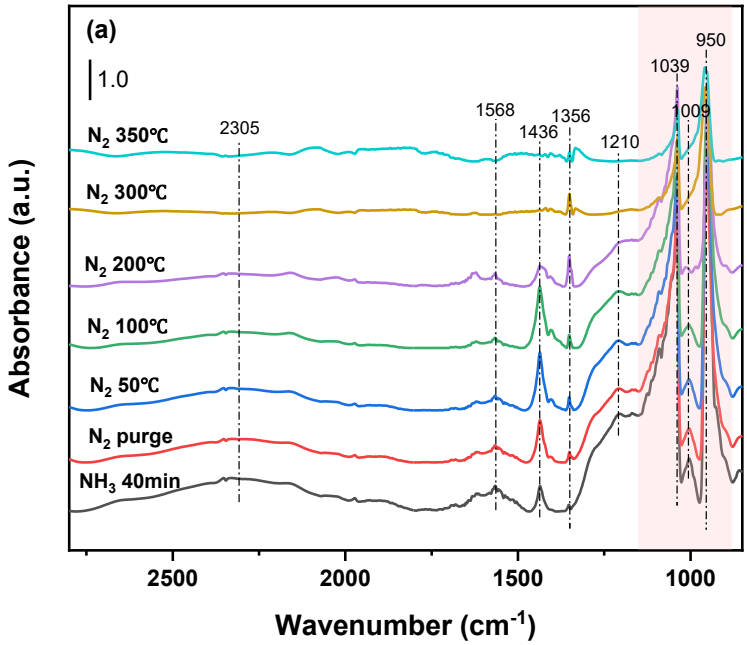
In the XPS spectrum of Ce 3d (Fig. 7c), the binding energies appeared at 881.0 (v_0), 885.0 (v'), 895.0 (u0) and 903.8 (u') were ascribed to Ce^{3+}. Whereas the remaining peaks , located at 882.8(v), 886.3 (v''), 899.8 (u), 913.9(u'') were ascribed to Ce^{4+}[29]. This indicates that both Ce^{3+} and Ce^{4+} coexist in all samples. As shown in Table 1, the $Ce^{4+}/(Ce^{3+}+Ce^{4+})$ ratio exhibits a volcano-shaped trend, reaching a maximum of 47% over the $2Ru/CeVO_4$ sample. The coexistence of Ce^{3+} and Ce^{4+} implies that the Ce^{4+}/Ce^{3+} redox couple remains available for redox cycling; meanwhile, the higher Ce^{4+} content in $2Ru/CeVO_4$ is accompanied by the largest O_α content, indicating that the variations in Ce^{4+} and O_α are synchronous. Similar to the O_α trend, the $3Ru/CeVO_4$ sample shows a reduced Ce^{4+} ratio (44%), which is consistent with the RuO_2 agglomeration evidenced and with the loss of Ru-$CeVO_4$ interfacial contact at

371 excessive loading.

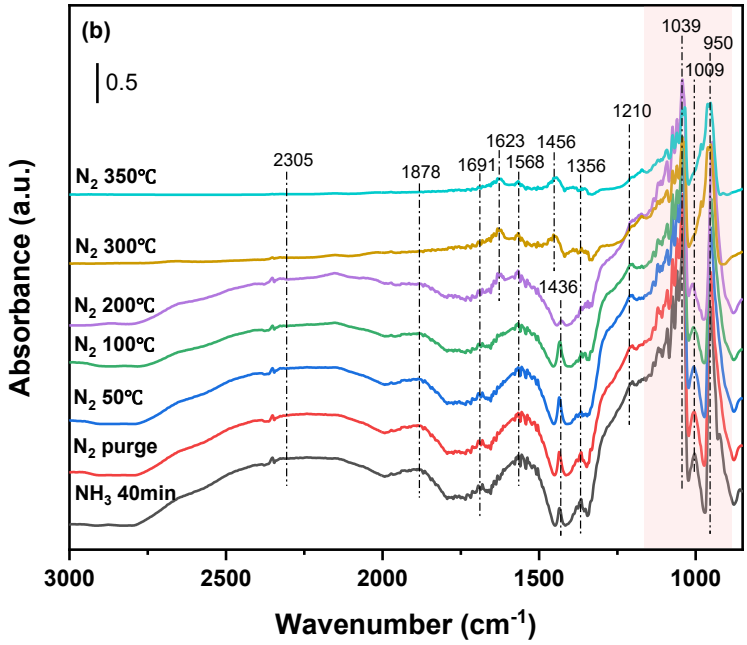
372 Fig. 7 (d) reveals the Ru 3d, C1s spectra in the as-prepared samples. The C1s peak was at
373 284.4 eV, which was attributed to carbonaceous contamination[30]. For all the reduced
374 samples, the Ru $3d_{5/2}$ peaks at 280.6 eV are observed, which was assigned to metallic Ru^{4+}
375 species in RuO_2[31]. Ru therefore exists on the calcined catalysts in an oxidised RuO_2, which
376 is consistent with the low-temperature H_2-TPR peak assigned to the reduction of RuO_2. The
377 Ru $3d_{5/2}$ intensity increases with the Ru loading, indicating a progressively higher surface
378 concentration of Ru; the fact that the activity does not increase further from 2 to 3 wt%
379 shows that it is the RuO_2 dispersion, and not the total amount of surface Ru, that governs the
380 performance. The RuO_2 species act as the sites at which NH_3 is dehydrogenated and
381 gas-phase O_2 is activated, and their optimal dispersion on $2Ru/CeVO_4$ accounts for its
382 superior NH_3-SCO activity.

383 **3.7 *In situ* DRIFT spectra Results**

384 **3.7.1 Adsorption of NH_3**


(a)
1.0
N2 350℃
N2 300℃
N2 200℃
N2 100℃
N2 50℃
N2 purge
NH3 40min
2305
1568
1436
1356
1210
1039
1009
950
Absorbance (a.a.)
2500
2000
1500
1000
Wavenumber (cm-1)

385


(b)
0.5
N2 350℃
N2 300℃
N2 200℃
N2 100℃
N2 50℃
N2 purge
NH3 40min
2305
1878
1691
1623
1568
1456
1436
1356
1210
1039
1009
950
Absorbance (a.a.)
3000
2500
2000
1500
1000
Wavenumber (cm-1)

386

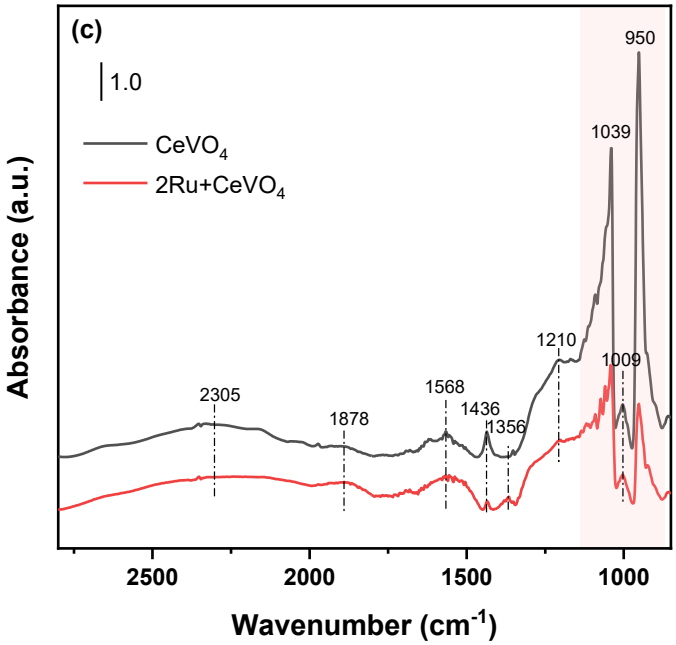


Fig. 8 *In situ* DRIFTs of the adsorption of NH_3 over (a) $CeVO_4$ and (b) $2Ru/CeVO_4$ catalysts at room temperature and successive purging with N_2 at various temperature. (c) Comparison diagram after 40 min of NH_3 introduction.

To elucidate the reaction pathway of NH_3 oxidation over the catalysts, *in situ* DRIFTs was employed to evaluate the possible mechanism of NH_3 oxidation. Initially, DRIFT spectra of NH_3 adsorption on $CeVO_4$ were recorded at room temperature and during subsequent N_2 purging at increasing temperatures, and are presented in Fig. 8(a). Following exposure of the sample to NH_3 for 40 min and subsequent N_2 purging, the bands observed at 1210 cm^{-1} and 1436 cm^{-1} were assigned to the symmetric bending vibration of NH_3 coordinated to Lewis acid sites and to the asymmetric bending vibration of NH_4^+ species on Brønsted acid sites, respectively[32-33]. The band at 1568 cm^{-1} is attributed to the scissoring vibration of weakly adsorbed NH_2 (amide) species, formed via the partial oxidation of NH_3 (H- abstraction)[34]. Additionally, a band at 2305 cm^{-1} was observed and can be assigned to the N-N stretching modes of adsorbed N_2O, a product arising from NH_3 oxidation[35]. Because this band,

together with the nitrate band at 1356 cm^{-1}[36], develops although no gas-phase O_2 is present, the oxidation of adsorbed NH_3 at this stage must proceed with the lattice oxygen of the catalyst, i.e. through a Mars-van Krevelen type participation of the $CeVO_4$ oxygen. Furthermore, the bands at 950, 1009, 1039 cm^{-1} might be related to NH_3 adsorption on VO_x species[37]. Notably, during the temperature-programmed N_2 purging process, the characteristic peaks ascribed to adsorbed NH_3 gradually vanished as the temperature rose above 300 ℃, and no new intermediate species were detected throughout the entire heating procedure. This indicates that the NH_3 adsorbed on pristine $CeVO_4$ is largely desorbed before it can be further dehydrogenated, in agreement with the NH_3-TPD result that the acid sites of $CeVO_4$ are only weakly developed. Although the lattice oxygen of $CeVO_4$ is able to oxidise a small fraction of the adsorbed NH_3, the amount of reactive oxygen supplied at low temperature is evidently insufficient to sustain the successive dehydrogenation of the surface NH_3, which is the main reason for the poor low-temperature NH_3-SCO activity of the support.

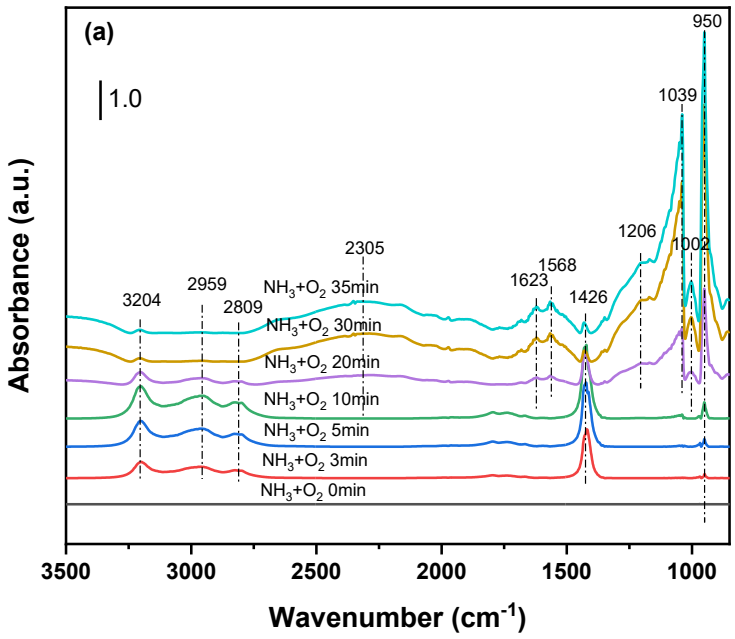
Fig. 8(b) presents the NH_3 adsorption-desorption infrared spectrum of 2Ru/$CeVO_4$ catalyst, and the peaks at 950, 1009, 1039, 1210, 1356, 1436, 1568 and 2305 cm^{-1} were all similar to those observed for $CeVO_4$. However, new characteristic peaks were also observed on the surface of 2Ru/$CeVO_4$. An additional band at 1691 cm^{-1}, assigned to the asymmetric bending vibration of NH_4^+ on Brønsted acid sites, was resolved after 40 min of NH_3 exposure, and the band at 1878 cm^{-1} was assigned to nitrosyl species (Ru-NO) formed on the Ru sites[38-39]. Upon heating, in contrast to the complete disappearance of characteristic peaks observed for $CeVO_4$, the peaks of 2Ru/$CeVO_4$ undergo a complex dynamic evolution accompanied by

notable frequency shifts. The bands ascribed to Brønsted acid sites and reactive intermediates are progressively depleted, while new bands concurrently emerge at 1456 and 1623 cm^{-1}, which are assigned to monodentate nitrate and bridging nitrate species[40-41]. Since no gas-phase O_2 is present during this step, the nitrate species can only be generated from the lattice oxygen of the catalyst, which directly demonstrates that the Ru-$CeVO_4$ interface markedly accelerates the supply of lattice oxygen. These results indicated that, upon heating, the adsorbed NH_3 could be activated to form -NH_2 intermediates through the abstraction of hydrogen. Accordingly, -NH would be formed from the continuous dehydrogenation as the temperature increased[38]. However, no obvious band assigned to -NH was observed, perhaps because the -NH reacted quickly with the lattice oxygen of 2Ru/$CeVO_4$, whose mobility is strongly enhanced by the Ru-O-V and Ru-O-Ce interfaces.

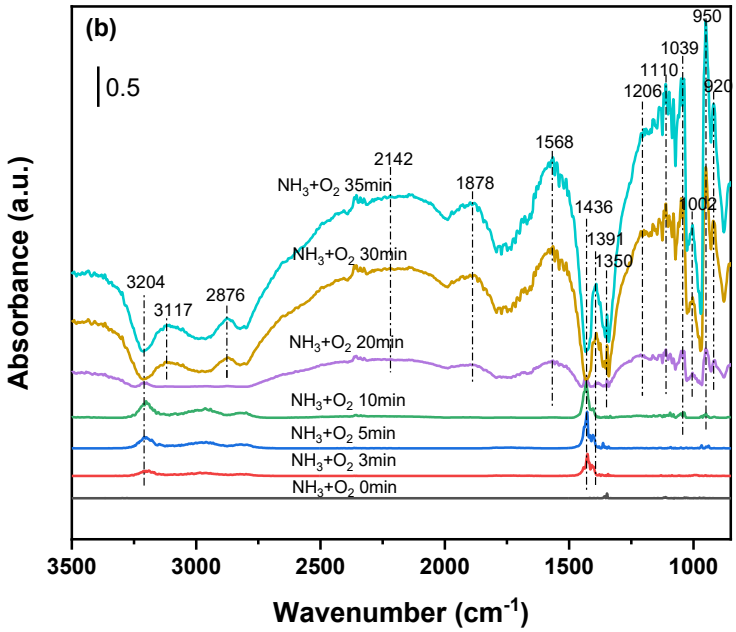
Further comparison of the spectral variations of the two catalysts following 40 min of NH_3 adsorption (Fig. 8c) shows that the relative band intensities differ markedly between the two samples. Upon introduction of Ru species, the bands assigned to Brønsted acid sites and reactive intermediates are markedly intensified, whereas those in the 900-1039 cm^{-1} region are significantly attenuated. In addition, as also observed in Fig. 8b, the residual 900-1039 cm^{-1} bands of 2Ru/$CeVO_4$ persist to higher temperatures, which indicates that the NH_3 coordinated to the VO_x sites is largely unreactive, while the dehydrogenation proceeds on the newly created Ru-related sites. Collectively, these variations in band intensity point to the existence of a strong metal-support interaction (SMSI) between Ru and the $CeVO_4$ support, which promotes the formation of Ru-O-V and Ru-O-Ce bonds and effectively modifies both the electronic structure and the density of acid sites on the catalyst surface. Through the

446 construction of efficient redox cycles involving Ru^{4+}/Ru^{2+}, V^{5+}/V^{4+}, and Ce^{4+}/Ce^{3+} couples,
447 as identified by XPS, the energy barrier for the surface dehydrogenation conversion of NH_3
448 is substantially lowered, thereby enabling the rapid transformation of physically adsorbed
449 NH_3 into highly reactive amide or imine intermediates. Concurrently, Ru facilitates the swift
450 migration of surface lattice oxygen to the active reaction sites, ensuring that the reactive
451 intermediates are oxidised at relatively low temperatures. Consequently, the $2Ru/CeVO_4$
452 catalyst exhibits a much higher low-temperature NH_3 conversion than pristine $CeVO_4$; it
453 should be stressed, however, that this faster surface oxidation is also responsible for its lower
454 N_2 selectivity, since the deep oxidation of the intermediates simultaneously produces N_2O
455 and NO_x.

456 **3.7.2 Adsorption of NH_3+O_2**



457



458

459 **Fig. 9** *In situ* DRIFTs of NH_3+O_2 at room temperature on $CeVO_4$ (a) and 2Ru/$CeVO_4$ (b)

460 catalysts.

461 The *in situ* DRIFTs spectra presented in Fig. 9(a) and (b) depict the evolution of surface

462 adsorbed species on $CeVO_4$ and 2Ru/$CeVO_4$ catalysts, respectively, upon exposure to a

463 flowing NH_3+O_2 gas mixture at room temperature over a time course from 0 to 35 minutes.

464 As for the $CeVO_4$ catalyst, the NH_3+O_2 adsorption with time was carried out via *in situ*

465 DRIFTs at room temperature (Fig. 9a). Several bands were clearly observed which were

466 attributed to NH_4^+ species adsorbed on Brønsted acid sites (1426 cm^{-1}) and to the N-H

467 stretching vibrations of coordinated NH_3 (2800-3204 cm^{-1}) after the catalyst sample exposed

468 into NH_3+O_2. The bands at 950-1039 cm^{-1} were ascribed to NH_3 adsorption on VO_x species

469 were detected as the reaction progress and the corresponding intensity gradually increased

470 with time elapsing. Furthermore, as the reaction time was prolonged, no noticeable shift or

471 intensity increase was observed for the characteristic peaks corresponding to the intermediate

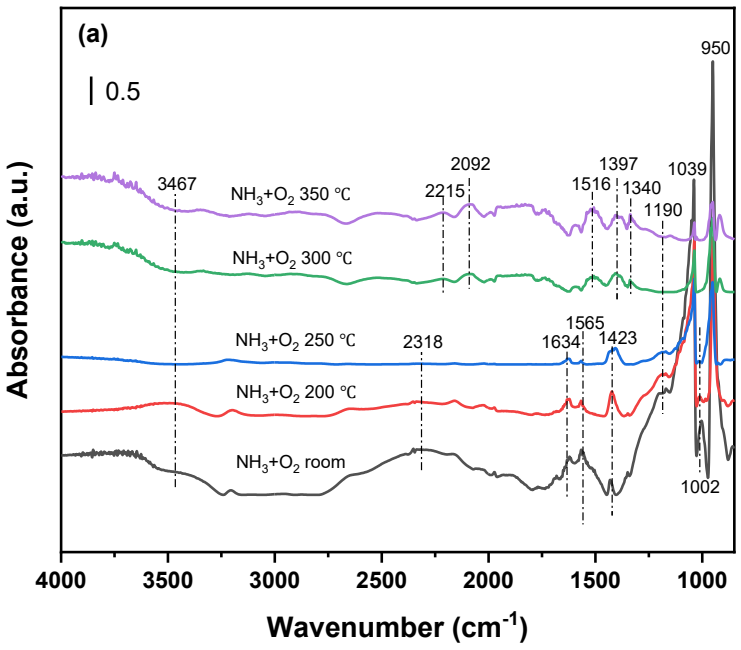
472 species -NH_2 (1563 cm^{-1}), nitrate (1623 cm^{-1}), and N_2O (2305 cm^{-1}). These weak features are

already present at the beginning of the exposure and remain unchanged, i.e. the small amount of oxidised species that $CeVO_4$ is able to generate from its own lattice oxygen (Fig. 8a) is not further increased by the addition of gas-phase O_2 at room temperature. This indicates that, although a certain number of active sites for NH_3 adsorption exist on the surface of pristine $CeVO_4$, the reaction between adsorbed NH_3 and O_2 proceeds extremely sluggishly at room temperature. This is primarily due to insufficient surface reactivity and poor lattice oxygen mobility, in agreement with the fact that the low-temperature H_2 consumption peak of $CeVO_4$ lies at the highest temperature among all the samples, which restrict the adsorbed ammonia predominantly to coordinated and physical adsorption states, rather than allowing it to overcome the energy barrier for NH_3 activation and dehydrogenation. Consequently, the transformation into key reactive intermediates is precluded. This accounts for the major reason behind the poor catalytic performance of pristine $CeVO_4$ in the low-temperature NH_3-SCO reaction.

In contrast, the spectral evolution of the $2Ru/CeVO_4$ catalyst depicted in Fig. 9(b) exhibits distinctly different characteristics. Upon introduction of NH_3 and O_2, similar adsorption peaks to those observed over $CeVO_4$ appear at 2800-3204, 2142, 1568, and 1437 cm^{-1}. However, marked differences are evident in both the adsorption intensities and the time scale of the reaction progression. After only 20 min of gas feeding, the reaction proceeds rapidly, with the peaks assigned to $-NH_2$ (1568 cm^{-1}) showing significantly higher intensities than those over pristine $CeVO_4$, while the band at 2142 cm^{-1} grows continuously. This indicates that the incorporation of Ru substantially promotes the activation and conversion of NH_3 at low temperatures. Meanwhile, with increasing reaction time, the peaks ascribed to Brønsted

acid sites gradually diminish and eventually disappear, while new features emerge at 1350 and 1391 cm^{-1}, assignable to nitrates/nitrites, and at 1884 cm^{-1}, corresponding to nitrosyl species (Ru-NO) on the Ru sites[42]. The formation of N-O containing species already at room temperature shows that the over-oxidation of NH_3 starts on $2Ru/CeVO_4$ under conditions where the support is still inactive, which is the molecular origin of its lower N_2 selectivity. Meanwhile, the peaks in the range of 950-1110 cm^{-1} undergo severe distortion and broadening, accompanied by the appearance of a new peak at 1110 cm^{-1}. These spectral changes suggest that the incorporation of Ru may induce a structural perturbation of the $CeVO_4$ surface layer and promote the formation of a Ru-O-V interfacial architecture, in line with the unchanged $CeVO_4$ lattice parameters observed by XRD. Such an interface not only enhances the mobility of lattice oxygen on the $CeVO_4$ surface but also establishes electron transfer pathways between the Ru^{4+}/Ru^{2+} and V^{5+}/V^{4+} redox couples.

3.7.3 The Interaction of NH_3 with O_2



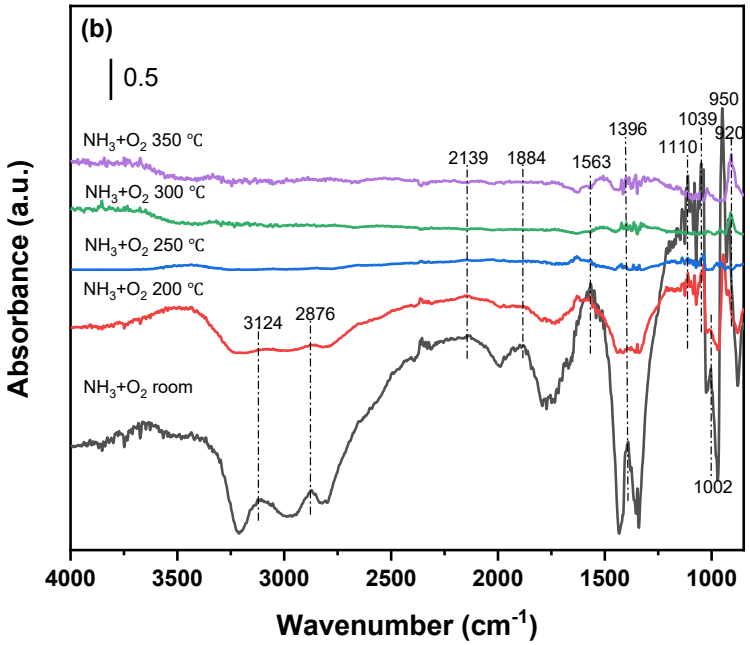


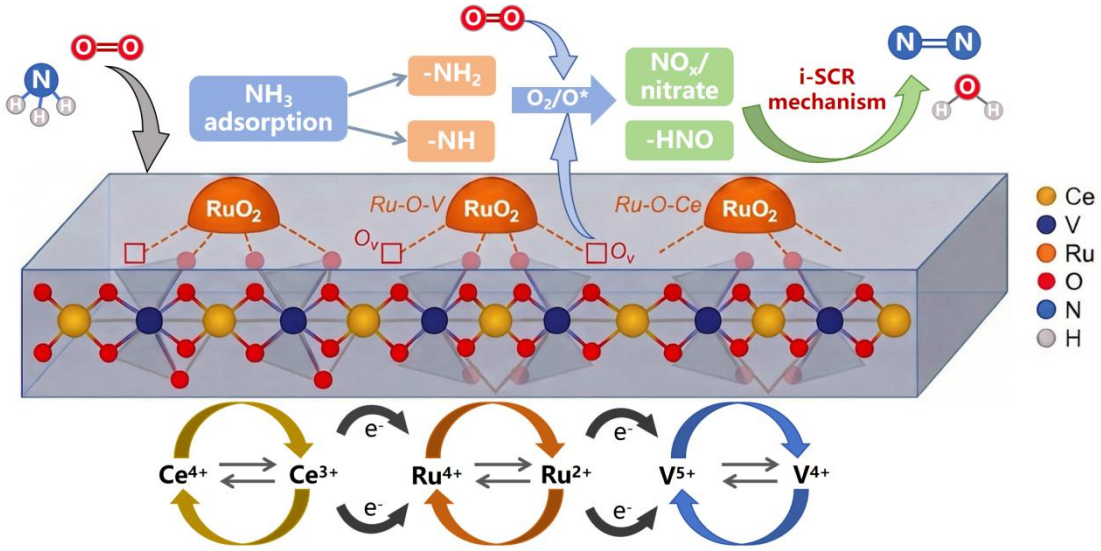
Fig. 10 *In situ* DRIFTs of NH_3+O_2 at different temperature on $CeVO_4$ (a) and 2Ru/$CeVO_4$ (b) catalysts.

To further investigate the reaction pathways of the two catalysts, *in situ* DRIFTs were acquired during temperature ramping under a feed of NH_3 and O_2, as shown in Fig. 10(a) and (b). For the pristine $CeVO_4$ catalyst shown in Fig. 10(a), the *in situ* DRIFTs within the lower temperature range from room temperature to 200 ℃ are predominantly characterized by vibrational bands attributed to nitrate species (1634 cm^{-1}), the reactive intermediate -NH_2 (1565 cm^{-1}), and N_2O (2318 cm^{-1}). However, upon elevating the reaction temperature to 300 ℃ and even 350 ℃, a pronounced spectral evolution occurs, with new absorption bands emerging at 2215, 2092, 1516, 1397, and 1340 cm^{-1}. Specifically, the peak at 2215 cm^{-1} is assignable to adsorbed N_2O generated from the oxidation of NH_3, whereas the band at 2092 cm^{-1} is consistent with a surface -NCO species; a series of intense bands at 1516, 1397, and 1340 cm^{-1} correspond to surface bidentate nitrates, monodentate nitrates, and nitrites, respectively. The emergence of these high-temperature species suggests that the pristine

$CeVO_4$ catalyst follows a sequential *i*-SCR pathway, in which the adsorbed NH_3 is first dehydrogenated to -NH_2 and then partly oxidised to surface NO_x/nitrate species that react with neighbouring NH_3 or -NH_2 to give N_2. The pronounced accumulation of nitrate and N_2O bands above 300 ℃ shows, however, that on $CeVO_4$ the reduction of these species is slower than their formation at high temperature, which is fully consistent with the activity data: although $CeVO_4$ retains the highest N_2 selectivity of the whole series at every temperature (95.7% at 240 ℃), its selectivity also drops markedly to 58.8% at 320 ℃.

For the 2Ru/$CeVO_4$ catalyst shown in Fig. 10(b), upon elevating the reaction temperature to 300 °C and even 350 °C, the characteristic bands of adsorbed NH_3 and reactive intermediates originally present on the catalyst surface essentially disappear, leaving the spectra nearly featureless with only extremely weak nitrate signals discernible at 1516 and 1397 cm^{-1}. Such a depletion of the surface species indicates that, at these temperatures, the consumption of the adsorbed NH_3 and of the N-containing intermediates is much faster than their replenishment, i.e. the surface reaction is no longer limited by the activation of NH_3. Based on the above analysis, the 2Ru/$CeVO_4$ catalyst exhibits a reaction pathway similar to that of the $CeVO_4$ counterpart, with both conforming to the typical "*i*-SCR" mechanism. The formation of Ru-O-V and Ru-O-Ce interfacial structures substantially enhances the catalyst's capability for O_2 activation and surface lattice oxygen transfer, thereby significantly boosting the NH_3 oxidation rate at low temperatures. However, as the temperature rises to 350 °C, the rates of NH_3 activation and oxidation on the catalyst surface become excessively high, such that the generated surface NO_x and nitrate intermediates cannot be timely consumed via reductive coupling with adjacent adsorbed NH_3 or -NH_2 species to form N_2. Instead, they are

546 released from the surface as gaseous nitrogen oxides, which is corroborated by the increase
547 of the NO_x and N_2O yields measured over $2Ru/CeVO_4$ (Fig. S1). This phenomenon
548 intrinsically reflects the ubiquitous activity-selectivity trade-off in NH_3-SCO reactions:
549 catalysts that accelerate low-temperature turnover often promote the over-oxidation of NH_3
550 to NO_x and N_2O byproducts at elevated temperatures. Consequently, despite the superior
551 catalytic activity exhibited by the $2Ru/CeVO_4$ catalyst in the low-temperature regime, its N_2
552 selectivity progressively deteriorates with increasing temperature, falling below that of
553 pristine $CeVO_4$ over the whole temperature range investigated (Fig. 11).



554

555 **Fig. 11** Reaction schematic diagram of $2Ru/CeVO_4$ catalyst in NH_3-SCO process.

556 **4. Conclusions**

557 In this study, a series of xRu/$CeVO_4$ (x = 0-3 wt%) catalysts were prepared by loading Ru
558 through aqueous impregnation on a $CeVO_4$ support synthesized by a microwave-assisted
559 deposition-precipitation method, and were evaluated for NH_3-SCO. The $2Ru/CeVO_4$ catalyst
560 achieved complete NH_3 conversion at 240 °C, whereas the bare $CeVO_4$ attained only 98.5%
561 conversion even at 320 °C, demonstrating the significant promotional effect of optimal RuO_x

loading on the low-temperature activity. From the experimental and characterization results, the following conclusions can be made:

(1) XRD and TEM characterization results showed that Ru species existed as highly dispersed amorphous nanoclusters on the $CeVO_4$ surface without disrupting the tetragonal zircon-type structure.

(2) NH_3-TPD and H_2-TPR and XPS results indicate that the incorporation of Ru enhanced surface chemisorbed oxygen (O_α) content, strengthened Lewis acid site density, and promoted Ce^{4+}/Ce^{3+} and V^{5+}/V^{3+} redox cycling, all of which collectively facilitated NH_3 adsorption, activation, and oxidation at low temperatures.

(3) Based on the detailed *in situ* DRIFTs studies the both catalysts followed the *i*-SCR mechanism, wherein adsorbed NH_3 was stepwise dehydrogenated to -NH_2 and -NH intermediates, which subsequently reacted with in situ generated NO_x/nitrate species to yield N_2. The Ru-O-V and Ru-O-Ce interfacial structures established efficient electron transfer pathways and accelerated lattice oxygen migration, accounting for the superior low-temperature performance of $2Ru/CeVO_4$. The same interfaces, however, also accelerate the over-oxidation of the surface intermediates, which explains why the N_2 selectivity of the Ru-containing samples is lower than that of the pristine support.

In summary, this work demonstrates that the incorporation of an optimal RuO_x loading (2 wt%) onto $CeVO_4$ support synergistically combines the high oxidation activity of RuO_x with the stable redox framework and acid site richness of $CeVO_4$, yielding a catalyst with markedly superior low-temperature NH_3-SCO activity compared to the bare support.

Declaration of Competing Interest

The authors declare that they have no known competing financial interests or personal relationships that could have appeared to influence the work reported in this paper.

Data availability

Data will be made available on request.

Acknowledgement

This work was supported by the State Key Laboratory Special Programs of China Minmetals Corporation (Grant No.2024GZGJ02) and Youth Science Fund Program of China Minmetals Corporation (Grant No.2026QNJJB28).

Supporting Information

Additional activity test (NH_3-SCO performance of $CeVO_4$ and *x*Ru/$CeVO_4$ catalysts. (a) NO_x yield and (b) N_2O yield.) and characterization data (SEM of $CeVO_4$ and 2Ru/$CeVO_4$) (PDF)

Reference

[1] Pan Y, Tian S, Liu D, Fang Y, Zhu X, Zhang Q, Zheng B, Michalski G, Wang Y (2016) Fossil fuel combustion-related emission dominate atmospheric ammonia sources during severe haze episodes: evidence from 15N-stable isotope in size-resolved aerosol ammonium. Environ Sci Technol 50:8049-8056. https://doi.org/10.1021/acs.est.6b00634.

[2] Kwon D, Park K, Hong S (2015) Influence of VO_x surface density and vanadyl species on the selective catalytic reduction of NO by NH_3 over VO_x/TiO_2 for superior catalytic activity. Appl Catal A 499:1-12. http://dx.doi.org/10.1016/j.apcata.2015.04.005.

[3] Gao FY, Liu YY, Sani Z, Tang XL, Yi HH, Zhao SZ, Yu QJ, Zhou YS (2021) Advances in selective catalytic oxidation of ammonia (NH_3-SCO) to dinitrogen in excess oxygen: A review on typical catalysts, catalytic performances and reaction mechanisms. J Environ Chem Eng 9:104575. https://doi.org/10.1016/j.jece.2020.104575.

[4] Liu JY, Sun MM, Lin QJ, Liu S, Xu HD, Chen YQ (2019) Promotional effects of ethylenediamine on the low-temperature catalytic activity of selective catalytic oxidation of ammonia over Pt/$SiAlO_x$:States and particle sizes of Pt. Appl Surf Sci 481:1344-1351. https://doi.org/10.1016/j.apsusc.2019.03.199

[5] Shin, YH, Kim, GJ, Hong SC (2020) Reaction properties of ruthenium over Ru/TiO_2 for selective catalytic oxidation of ammonia to nitrogen. Appl Surf Sci 506:144906. https://doi.org/10.1016/j.apsusc.2019.144906

[6] Zheng Z, Yang Y, Li H, Xin Q, Zhang S, Liu Y, Liu SJ, Zheng CH, Song H, Gao X (2020) Effect of multi-pollutant on the catalytic oxidation of dichloromethane over RuO_2-$WO_3/Sn_{0.2}Ti_{0.8}O_2$ catalyst. Fuel 278:118207.

https://doi.org/10.1016/j.fuel.2020.118207

[7] Zhang QL, Zhang TX, Xia FT, Zhang YQ, Wang HM, Ning P (2020) Promoting effects of acid enhancing on N_2 selectivity for selective catalytic oxidation of NH_3 over RuO_x/TiO_2: The mechanism study. Appl Surf Sci 500:144044. https://doi.org/10.1016/j.apsusc.2019.144044

[8] Hua ZS, Xin Q, Ren WJ, Zheng Z, Zhou FY, Liu SJ, Yang Y, Gao X (2022) Enhanced performance of Nb_2O_5 decorated $RuO_2/Sn_{0.2}Ti_{0.8}O_2$ for selective catalytic oxidation of ammonia. Chem Eng J 160:948-957. https://doi.org/10.1016/j.psep.2022.03.005

[9] Li S, Li J, Liang W, Cai J, Guo R (2024) Promoting effects of cerium oxide on catalysts performance for selectivity catalytic oxidation of NH_3 over RuO_x/TiO_2. J Environ Chem Eng 12:113528. https://doi.org/10.1016/j.psep.2022.03.005

[10] Zhao X, Huang L, Li HR, Hu H, Hu XN, Shi LY, Zhang DS (2016) Promotional effects of zirconium doped $CeVO_4$ for the low-temperature selective catalytic reduction of NO_x with NH_3. Appl Catal B 183:269-281. http://dx.doi.org/10.1016/j.apcatb.2015.10.052

[11] Gillot S, Tricot G, Vezin H, Dacquin JP, Dujardin C, Granger P (2017) Development of stable and efficient $CeVO_4$ systems for the selective reduction of NO_x by ammonia: Structure-activity relationship. Appl Catal B 218:338-348. http://dx.doi.org/10.1016/j.apcatb.2017.06.049

[12] Li YY. Zhang ZP, Zhang TR, Jiang QY, Niu XY, Zhu YJ (2024) Engineering the surface properties of $CeVO_4$ catalysts to improve low temperature De-NO_x performance through regulating pH value in synthesis process. Fuel 362:130836. https://doi.org/10.1016/j.fuel.2023.130836

642 [13] Li SY, Song LY, Li J, Hong H (2023) Promotional Mechanisms of Activity and SO_2
643 tolerance of $NdVO_x/TiO_2$ Catalysts for Selectivity Catalytic Reduction of NO_x with NH_3.
644 ACS Catal 13:2867-2884. https://doi.org/10.1021/acscatal.2c06338
645 [14] Zhang AC, Zhang ZH, Lu H, Liu ZC, Xiang J, Zhou CS, Xing WB, Sun LS (2015)
646 Effect of promotion with Ru addition on the activity and SO_2 resistance of MnO_x-TiO_2
647 adsorbent for Hg^0 removal. Ind Eng Chem Res 54:2930-2939.
648 https://doi.org/10.1021/acs.iecr.5b00211
649 [15] Busca G, Lietti L, Ramis G, Berti F (1998) Chemical and mechanistic aspects of the
650 selective catalytic reduction of NO_x by ammonia over oxide catalysts: A review. Appl Catal B
651 18:1-36. https://doi.org/10.1016/j.cej.2024.150374
652 [16] Jiang ZX (2025) Promotional catalytic activity of bifunctional Ru-Ce-Zr catakysts for
653 NH_3-SCO by deposition order of dual active components. Catal Lett 155:45.
654 https://doi.org/10.1007/s10562-024-04891-9
655 [17] Tian Y, Han ZT, Zhao HZ, Zeng QL, Li YS (2024) Enhancing acidity of $Ru/Ce/ZrO_2$
656 bifunctional catalysts for promoting N_2 Selectivity in selective catalytic oxidation of NH_3. J
657 Environ Chem Eng 12:113888. https://doi.org/10.1016/j.jece.2024.113888
658 [18] Li P, Xin Y, Li Q, Wang ZP, Zhang ZL, Zheng LR (2012) Ce-Ti amorphous oxides for
659 selective catalytic reduction of NO with NH_3: confirmation of Ce-O-Ti active sites. Environ
660 Sci Technol 46:9600-9605. https://dx.doi.org/10.1021/es301661r
661 [19] Zhao HZ, Han ZT, Cheng SS, Tian Y, Zeng QL, Li YS, Ma D (2024) Catalytic Activity
662 and reaction mechanism of Ru-modified $Ce_{0.7}Zr_{0.3}O_x$ catalysts for selective catalytic
663 oxidation of ammonia. Energy Fuels 38:22440-22449.

https://doi.org/10.1021/acs.energyfuels.4c03739

[20] Xu XH, Ling YC, Bi JY, Chen BA, Wang P, Li L, Wang XH, Fei ZY, Qiao X (2026) Rational design of Ru-CeO_2/Al_2O_3 composite catalysts: Insight into special catalytic behavior in dimethyl disulfide oxidation. Ind Eng Chem Res 65:3622-3633. https://doi.org/10.1021/acs.iecr.5c04383

[21] López-Rodríguez S, Davó-Quiñonero A, Bailón-García E, Lozano-Castelló D, Bueno-López A (2021) Effect of Ru loading on Ru/CeO_2 catalysts for CO_2 methanation. Mol Catal 515:111911. https://doi.org/10.1016/j.mcat.2021.111911

[22] Li YY, Zhang ZP, Zhang TR, Jiang QY, Niu XY, Zhu YJ (2024) Engineering the surface properties of $CeVO_4$ catalysts to improve low temperature De-NO_x performance through regulating pH value in synthesis process. Fuel 362:130836. https://doi.org/10.1016/j.fuel.2023.130836

[23] Agula B, Ren TZ, Zhao X, Zhaorigetu B, Yuan ZY (2011) Relationship between the reducibility and selectivity of $CeMo_xV_{1-x}O_4$ catalysts by kinetic parameters of TPR. J Nat Gas Chemistry 2011;20:232-236. https://doi.org/10.1016/S1003-9953(10)60182-X

[24] Tushar S, Leon L （2018）Structure-dependent activity of CeO_2 supported Ru catalysts for CO_2 methanation. J Catal 367:171-180. https://doi.org/10.1016/j.jcat.2018.08.027

[25] George A, Theophilos I （2006） Effect of synthesis parameters on catalytic properties of CuO-CeO_2. Appl Catal B 67:1-11. https://doi.org/10.1016/j.apcatb.2006.04.005

[26] Xia Y, Dai H, Zhang L, Deng J, He H, Chak T (2010) Ultrasound-assisted nanocasting fabrication and excellent catalytic performance of three-dimensionally ordered mesoporous chromia for the combustion of formaldehyde, acetone, and methanol. Appl Catal B

686 100:229-237. https://doi.org/10.1016/j.apcatb.2010.07.037

687 [27] Wu Z, Jin R, Liu Y, Wang H (2008) Ceria modified MnO_x/TiO_2 as a superior catalyst for
688 NO reduction with NH_3 at low-temperature. Catal. Commun 9:2217-2220.
689 https://doi.org/10.1016/j.catcom.2008.05.001

690 [28] Crist, B. V (1999) Handbook of the elements and native oxide, XPS; Inc. Mountain
691 View: CA, 80-82.

692 [29] Chen J, Chen X, Yan DX, Jiang MZ, Xu WJ, Yu H, Jia HP (2019) A facile strategy of
693 enhancing interaction between cerium and manganese oxides for catalytic removal of
694 gaseous organic contaminants. Appl Catal B 250:396-407.
695 https://doi.org/10.1016/j.apcatb.2019.03.042

696 [30] Li DL, Li RL, Lu MM, Lin XY, Zhan YY, Jiang LL (2017) Carbon dioxide reforming of
697 methane over Ru catalysts supported on Mg-Al oxides: A highly dispersed and stable
698 Ru/Mg(Al)O catalyst. Appl Catal B 200:566-577.
699 https://doi.org/10.1016/j.apcatb.2016.07.050

700 [31] Faroldi BM, Munera JF, Cornaglia LM. In situ characterization of phase transformation
701 and reactivity of high surface area lanthanum-based Ru catalysts for the combined reforming
702 of methane. Appl Catal B 150-151:126-137. https://doi.org/10.1016/j.apcatb.2013.12.005

703 [32] Chen LA, Li JH, Ge MF. DRIFT study on cerium-tungsten/titiania catalyst for selective
704 catalytic reduction of NO_x with NH_3. Environ Sci Technol 44:9590-9596.
705 https://doi.org/10.1021/es102692b

706 [33] Han LP, Gao M, Hasegawa J, Li SX, Shen YJ, Li HR, Shi LY, Zhang DS (2019)
707 SO_2-tolerant selectivity catalytic reduction of NO_x over Meso-TiO_2@ Fe_2O_3 @ Al_2O_3

metal-based monolith catalysts. Environ Sci Technol 53:6463-6473. https://doi.org/10.1021/acs.est.9b00435

[34] Liu FD, He H, Zhang CB, Shan WP, Shi XY (2011) Mechanism of the selective catalytic reduction of NO_x with NH_3 over environmental-friendly iron titanate catalyst. Catal Today 175:18-25. https://doi.org/10.1016/j.cattod.2011.02.049

[35] Amores JMG, Escribano VS, Ramis G, Busca G (1997) An FT-IR study of ammonia adsorption and oxidation over anatase-supported metal oxides. Appl Catal B 13:45-58. https://doi.org/10.1016/S0926-3373(96)00092-6

[36] Yang SJ, Guo YF, Chang HZ, Ma L, Peng Y, Qu Z, Yan NQ, Wang CZ, Li JH (2013) Novel effect of SO_2 on the SCR reaction over CeO_2: Mechanism and significance. Appl Catal B 136-137:19-28. https://doi.org/10.1016/j.apcatb.2013.01.028

[37] Mu JC, Li XY, Sun WB, Fan SY, Wang XY, Wang L, Qin MC, Gan GQ, Yin ZF, Zhang DK (2018) Inductive Effect Boosting catalytic performance of advanced $Fe_{1-x}V_xO_\sigma$ catalysts in low-temperature NH_3 selective catalytic reduction: Insight into the structure, Interaction, and mechanisms. ACS Catal 8:6760-6774. https://doi.org/10.1021/acscatal.8b01196

[38] Zhang L, He H (2009) Mechanism of Selective catalytic oxidation of ammonia to nitrogen over Ag/Al_2O_3. J Catal 268:18-25. https://doi.org/10.1016/j.jcat.2009.08.011

[39] Chen WM, Ma YP, Qu Z, Liu QH, Huang WJ, Hu XF, Yan NQ (2014) Mechanism of the selective catalytic oxidation of slip ammonia over Ru-Modified Ce-Zr complexes determined by in situ diffuse reflectance infrared fourier transform spectroscopy. Environ Sci Technol 48:12199-12205. https://doi.org/10.1021/es502369f

[40] Chen WM, Qu Z, Huang WJ, Hu XF, Yan NQ (2016) Novel effect of SO_2 on selective

730 catalytic oxidation of slip ammonia from coal-fired flue gas over IrO_2 modified Ce-Zr solid
731 solution and the mechanism investigation. Fuel 166:179-187.
732 https://doi.org/10.1016/j.fuel.2015.10.116
733 [41] Wang F, He GZ, Zhang B, Chen M, Chen XY, Zhang CB, He H (2019) Insights into the
734 activation effect of H_2 pretreatment on Ag/Al_2O_3 catalyst for the selective oxidation of
735 ammonia. ACS Catal 9:1437-1445. https://doi.org/10.1021/acscatal.8b03744
736 [42] Ma L, Seo CY, Nahata M, Chen XY, Li JH, Schwank JW. Shape dependence and sulfate
737 promotion of CeO_2 for selective catalytic reduction of NO_x with NH_3. Appl Catal B
738 232:246-259. https://doi.org/10.1016/j.apcatb.2018.03.065

Supplementary Files

This is a list of supplementary files associated with this preprint. Click to download.

- supportinginformation.docx